Role of crystal structure on CO_2 capture by limestone derived CaO subjected to carbonation/recarbonation/calcination cycles at Ca-looping conditions

J. M. Valverde[a], P. E. Sanchez-Jimenez[b], L. A. Perez-Maqueda[b], M. A. S. Quintanilla[a], J. Perez-Vaquero[a]

[a] Faculty of Physics. University of Seville. Avenida Reina Mercedes s/n, 41012 Sevilla, Spain

[b] Institute of Materials Science (C.S.I.C.-Univ. Seville) Americo Vespucio 49, 41092 Sevilla, Spain.

(Dated: February 18, 2014)

Abstract

Large scale pilot plants are currently demonstrating the feasibility of the Calcium-looping (CaL) technology built on the multicyclic calcination/carbonation of natural limestone for post-combustion and pre-combustion CO_2 capture. Yet, limestone derived CaO exhibits a drop of conversion when subjected to multiple carbonation/calcination cycles, which lessens the efficiency of the technology. In this paper we analyze a novel CaL concept recently proposed to mitigate this drawback based on the introduction of an intermediate stage wherein carbonation is intensified at high temperature and high CO_2 partial pressure. It is shown that carbonation in this stage is mainly driven by solid-state diffusion, which is determined by the solid's crystal structure. Accordingly, a reduction of crystallinity by ball milling, which favors diffusion, serves to promote recarbonation. Conversely, thermal annealing, which enhances crystallinity, hinders recarbonation. An initial fast phase has been identified in the recarbonation stage along which the rate of carbonation is also a function of the crystal structure indicating a relevant role of surface diffusion. This is consistent with a recently proposed mechanism for nucleation of $CaCO_3$ on the CaO surface in islands with a critical size determined by surface diffusion. A further issue analyzed has been the effects of pretreatment and cycling on the mechanical strength of the material, whose fragility hampers the CaL process efficiency. Particle size distribution of samples dispersed in a liquid and subjected to high energy ultrasonic irradiation indicate that milling promotes friability whereas thermal annealing enhances the resistance of the particles to fragmentation even though pretreatment effects become blurred after cycling. Our study demonstrates that recarbonation conditions and crystal-structure controlled diffusion are important parameters to be considered in order to assess the efficiency of CO_2 capture in the novel CaL concept.

* **Corresponding author at:** Department of Electronics and Electromagnetism, Faculty of

Physics, Avda. Reina Mercedes s/n, 41012 Seville (Spain). Phone no. +34 954550960. Fax no. +34 954239434. Email: jmillan@us.es

I. INTRODUCTION

The multicyclic carbonation/decarbonation of CaO plays a central role on an increasing number of emerging technologies focused on CO_2 capture [1–3]. The efficiency of the so-called Ca-looping (CaL) technology has been successfully demonstrated in pilot-scale tests based on a dual gas-solid fluidized bed reactors system [4]. CaO solid particles are carbonated in a fluidized bed reactor at contact with the inlet gas containing a low concentration of CO_2 (typically around 15% vol in postcombustion gas) after which the partially carbonated particles are circulated into a second reactor where decarbonation takes place by calcination. In the calciner, a stream of CO_2 is released for storage while CaO particles are regenerated to be used in a new cycle. Due to practical constraints imposed for post-combustion CO_2 capture (such as short residence times, low CO_2 concentration for carbonation and high CO_2 concentration in the calciner) and taking into account the tradeoff between the reaction kinetics and equilibrium driving force, carbonation is carried out at temperatures around 650°C whereas calcination requires temperatures above 850°C [1].

Thermogravimetric analysis (TGA) tests have demonstrated that carbonation of CaO progresses through two well differentiated phases [5, 6]. The CaO skeleton is partially carbonated in a first kinetically-controlled fast phase until a 30-50 nm thick layer of $CaCO_3$ is built up on the solid's surface. From this point, carbonation proceeds at a much slower rate. Early TGA tests reported by Bhatia and Perlmutter [7] indicated that this slow phase would be controlled by the solid-state diffusion of CO_3^{2-} mobile ions through the $CaCO_3$ product layer and counter-current diffusion of O^2- anions to maintain electro-neutrality as recently confirmed by direct experimental observations using inert markers [8]. Anyhow, carbonation at ordinary CaL conditions takes place mostly in the fast phase whereas diffusive carbonation

is not significant due to short residence times. The efficiency of the CaL technology is thus mostly determined by the regenerability of CaO surface area in the calcination stage of each cycle.

Due to its low cost and wide availability, natural limestone stands as the most suitable CaO precursor to guarantee the industrial competitiveness of the CaL technology [9, 10]. Yet, the porous CaO skeleton derived from rapid calcination of raw limestone is prone to suffer severe sintering mainly because of lattice diffusion at the high temperatures reached during calcination [11, 12]. As a consequence, the sorbent surface area suffers a progressive reduction with the cycle number, which is accompanied by an irreversible loss of CaO conversion (grams of CaO carbonated/grams of CaO initial). Only after a large number of cycles CaO conversion converges asymptotically to a stable but quite small residual value [13–15]. The drastic loss of conversion (along with the irreversible sulphation of CaO in postcombustion applications) makes it necessary to continuously purge a fraction of sorbent while replacing it with fresh limestone in order to achieve a sustained high level of CO_2 capture efficiency, which increases the demand of heat in the calciner and the overall cost of the process [16–18].

Introducing a recarbonation stage between carbonation and calcination has been proposed as a practically feasible procedure to attenuate the rate of limestone deactivation and increase its residual conversion [19–21]. Accordingly, a novel CaL concept is based on further carbonating the partially carbonated particles in an intermediate reactor operated at high temperature (around 800°C) and high concentration of CO_2 available from the calciner. Upon calcination of the recarbonated sorbent, CO_2 escaping from the solid inward skeleton would leave behind a regenerated CaO sorbent with enhanced porosity and surface area [22].

The evolution of the sorbent when subjected to multiple carbonation/calcination cycles has a great influence on the efficiency of the CaL technology derived from process simu-

lations and economic analysis [9, 16, 20, 21, 23, 24]. In particular, solid-state diffusion, which is basically determined by the crystal structure [25], is expected to play an important role on the effect of recarbonation on the multicyclic sorbent behavior. A goal of the present work is to study the influence of crystal structure on the conversion of CaO along carbonation/recarbonation/calcination cycles. To this end, the behavior of limestone samples presubjected to diverse treatments modifying the solid crystal structure will be investigated. On one hand, we will analyze the response of a limestone previously subjected to ball milling, which gives rise to a high density of structural defects in the crystal lattice that would act as fast diffusion pathways [26, 27]. On the other hand, we will look at the effect of a prolonged heat treatment of limestone in CO_2 (at 850°C to avoid decomposition). This thermal treatment (annealing) promotes lattice diffusion, which leads to an improvement of crystallinity by reducing the density of dislocations and defects [28]. The resistance of a thermally annealed sample to diffusion would be thus enhanced as reported in several works [29, 30]. A further issue that besets the use of natural limestone particles in the CaL technology is their marked friability, which leads to high attrition rates and material losses by elutriation of very fine fragments [1, 31]. In our work, the mechanical strength of the pretreated limestones will be analyzed by looking at the particle size distribution of samples dispersed in a liquid and subjected to high energy ultrasonic irradiation [32]. Local shear stresses of huge intensity generated by ultrasonication may cause attrition to a great extent of low strength materials [33] such as limestone as seen from high speed photography showing that cavitation phenomena causes local stresses sufficiently high as to fragment the particles [34]. As will be seen, fragmentation is enhanced in previously milled limestone, which indicates its relatively low strength whereas it is otherwise in the case of the thermally annealed material. Moreover, the effect of carboantion/recarbonation/calcination cycles on

the mechanical strength of the particles has been analyzed.

II. MATERIALS AND METHODS

The material used in our study is a natural limestone (Matagallar quarry at Pedrera, Spain) of high purity (99.62% $CaCO_3$, $SiO_2 < 0.05\%$, $Al_2O_3 < 0.05\%$, 0.24% MgO, 0.08% Na_2O). The performance as CO_2 sorbent and characterization of this limestone were investigated as affected by two diverse pretreatments consisting of annealing by prolonged isothermal heating (850°C for 12 h in a CO_2 atmosphere) and ball milling. In the latter, 6.5 g of limestone were milled in a 100 cm^3 steel jar with 200 tungsten carbide balls (5.5 mm in diameter) operated in a centrifugal ball-mill (Fritsch Pulverisette 6, centrifugal version, Idar-Oberstein, Germany) at 500 rpm for 1 hour. Limestone-to-ball mass ratio was set at 1:40.

Scanning Electron Microscopy (SEM) analysis was made by using a HITACHI Ultra High-Resolution S-5200 equipped with a EDX spectroscopy unit (Bruker AXS Microanalysis GmbH). Further imaging analysis was conducted by means of a modular Scanning Probe Microscope (SPM) system (Molecular Imaging Pico Plus) using AppNano ACT silicon tapping-mode rectangular cantilevers, which allowed us to obtain 3D images of the particles' top surface. To this end, a powder sample was firstly deposited on either a freshly cleaved mica or polydimethylsiloxane (PDMS) substrate after which it was gently tapped to obtain a dispersed layer of small agglomerates. The cantilever tip was placed close to a group of particles using an auxiliary top-view optical microscope. The sample was then approached in tapping mode and an image of a small area of the surface (typically 4 x 4 micrometers) was obtained. In most cases, the area imaged contained no particles. If so, the scan area was enlarged until a particle or group of particles were located. The next step

was to re-center and resize the scan area in order to box the particles as tight as possible. Slow scan rates (typically 1 line/second or slower) were applied in order not to displace the particles. Once the scan area was centered on the particle, the imaging parameters (scan rate, gains and setpoint) were tuned to optimize the image of the particles apex.

X-ray diffraction (XRD) analysis was performed using a Bruker D8 Advance powder diffractometer equipped with a high temperature chamber in order to measure crystallinity and crystal coherence length of raw, milled and thermally annealed limestone samples at ambient conditions, after calcination at 850°C in air and subsequent recarbonation under CO_2 at 650°C in-situ.

Particle size distributions have been obtained using a Mastersizer 2000 instrument (Malvern Instruments), which measures particle size by means of laser diffractometry according to the international standard for laser diffraction measurements ISO13320-1. Powder samples are pre-dispersed in a liquid to decrease their surface energy, which helps de-agglomeration. In our work, 2.5 g of powder sample was added to 100 ml of 2-propanol, which according to the international standard for laser diffraction measurements ISO 14887 is a suitable dispersant for $CaCO_3$ particles at this optimum concentration level. The wet sample pre-dispersion unit employed was the Hydro 2000S, which comprises an electric motor that drives a stirrer and impeller in the dispersion tank to provide a simultaneous stirring and pumping action that moves the agitated sample via the sample tubing to the measuring cell located in the optical bench. The effect of pretreatment on the mechanical strength of limestone has been studied by measuring the particle size distributions (PSDs) of liquid dispersions previously subjected to high energy ultrasonic irradiation (150 W/dm^3, 40 kHz) for 10 min able to cause particle fragmentation.

Multicyclic CaO conversion of samples subjected to carbonation/recarbonation/calcination

(c/r/c) cycles was analyzed by means of thermogravimetric analysis (TGA) tests, which were carried out using a Q5000IR TG analyzer (TA Instruments). This instrument is provided with an infrared furnace heated by halogen lamps and a high sensitivity balance (<0.1 μg) characterized by a minimum baseline dynamic drift (<10 μg). The infrared halogen furnace helps fast heating/cooling of the sample, which allows mimicking the sudden change of temperature suffered by the sorbent in practice as it is rapidly circulated between different reactors at diverse temperatures. As a general initialization procedure, the limestone sample (of mass $\simeq$10 mg) was firstly heated in-situ by a linear program (20°/min) up to 850°C in dry air for decarbonation after which it was subjected to the c/r/c cycles. Benchmark conditions consisted of carbonation at 650°C (85% dry air/15% CO_2 vol/vol) for 5 min, recarbonation at 800°C (10% dry air/90% CO_2 vol/vol) for 3 min and calcination at 850°C (dry air) for 5 minutes. The heating/cooling rates between these stages was set to 300°C/min.

III. EXPERIMENTAL RESULTS AND DISCUSSION

A. SEM/SPM analysis

Representative SEM images of raw, milled and thermally annealed samples are displayed in Fig. 1 showing a clear effect of pretreatment on the textural features of the particles' surface. Raw limestone particles appear as irregularly shaped (as expected since they are produced by limestone rock crushing) with a certain presence of small fragments (Fig. 1a). Fragmentation and surface irregularities become the dominant pattern in the images obtained for the milled sample (Fig. 1b). On the other hand, limestone particles would suffer severe sintering by heat treatment at 850°C, which is well above the Tamman temperature

for $CaCO_3$ ($\sim$533°C) [35]. The Tamman temperature, which is about 1/2 of the melting temperature (in °K) marks the point at which atoms in the bulk become to exhibit an appreciable mobility, and this will lead to sintering. Moreover, sintering is further intensified by the presence of CO_2, which further enhances surface diffusion [11, 36]. Accordingly, relatively larger and highly sintered particles with smooth surfaces are seen in SEM images of the thermally annealed sample (Fig. 1c). A distinctive feature observed in these images is the growth of single nanocrystals on the particles' surface (see Fig. 2 for a higher magnification picture) with a typical size $\sim$50 nm. In some cases, a trigonal crystal structure is clearly identifiable as characteristic of calcite single crystals. EDS analysis was carried out to confirm that the composition of these nanocrystals conformed to $CaCO_3$. SPM 3D images are shown in Fig. 3 further illustrating fragmentation and surface damage caused by milling as well as enhanced sintering provoked by thermal annealing. Single nanocrystals scattered on the surface of thermally annealed particles are also visible in SPM images (see Fig. 3c and Fig. 2).

B. XRD analysis

Figure 4a shows XR diffractograms measured for raw, milled and thermally annealed limestone samples in air at ambient temperature. XR diffractograms obtained after calcination in-situ (increasing the temperature at a rate of 20°/C up to 850°C in air) and after in-situ recarbonation (quickly decreasing the temperature down to 650°C and introducing CO_2 at 1 bar for 20 min) are plotted in Fig. 4b and Fig. 4c, respectively. Figure 5 displays the degree of crystallinity (crystallinity % as determined by XRD pattern analysis) and coherent crystal length L obtained from the Scherrer equation and the X-ray line broadening at half the maximum intensity (FWHM).

As expected, crystallinity % and coherent crystal length of the limestone samples tested at ambient conditions are notably affected by the type of pretreatment. Thermal annealing enhances crystallinity % and coherent crystal length (which turns out to be around 60nm and similar to the size of single nanocrystals observed in the SEM/SPM images) whereas milling leads to the opposite effect (as well known from studies about the effect of milling on the crystal structure of solids [37]). The structure damaged by milling is healed by calcination as inferred from Fig. 5 by the increase of the coherent crystal length, which can be explained as due to the promoted mobility of atoms in the solid. Atoms at crystal defects become mobile when the Huttig temperature T_H is reached, which is about 1/3 of the melting temperature (in °K). Taking into account the melting temperatures of CaO and $CaCO_3$ (about 2610°C and 1330°C, respectively [38]) it is $T_H \simeq 690$°C for CaO whereas the Huttig temperature is much lower for $CaCO_3$ ($T_H \simeq 260$°C) even though other factors such as particle size and morphology will be also determinant. On the other hand, calcination is seen to cause a drop of the coherent crystal length of the raw and annealed limestones (Fig. 5), which is specially marked in the latter case. In regards to the crystallinity % of these raw and annealed samples, it remains almost constant after calcination but a noticeable decrease is observed upon recarbonation. This observation would be in accordance with the remarkably small activation energies reported elsewhere [39] for diffusion through the $CaCO_3$ product layer formed by carbonation of CaO perfect crystals (as compared with activation energies for diffusion in single $CaCO_3$ crystals). As suggested in [39] and demonstrated by our XRD analysis, this could be explained by a reduced degree of crystallinity of the recarbonated structure. Thus, the XRD analysis indicates that the influence of pretreatment on the crystal structure becomes blurred after recarbonation yielding similar degrees of crystallinity and coherent crystal length for the three samples. Even though in-situ recarbonation in the

XRD chamber (carried out under pressurized CO_2 and for a long period of time) does not mimic exactly CaL conditions, this result suggests that the effect of pretreatment on the multicyclic conversion of these sorbents would fade away after a number of recarbonations at high CO_2 partial pressure.

According to a recent theoretical study on the carbonation of single CaO crystals [40], a possible effect of pretreatment on the relative growth of (1,0,0) and (1,1,1) CaO oriented surfaces might have a decisive influence on the carbonation reactivity. Chemisorption of CO_2 molecules on these surfaces was examined in that work by evaluating the energy change associated with $CaCO_3$ nucleation. The analysis concludes that $CO_2 + O \rightarrow CO_3$ substitutions on O sites of (1,1,1) surfaces of CaO perfect crystals is the most likely mechanism for carbonation whereas CaO (1,0,0) surfaces are unfavorable for CO_2 insertion. Figure 4b shows however that the relative intensity of the diffraction peaks corresponding to the (1,1,1) and (2,0,0) planes of CaO resulting from calcination is essentially independent of the type of pretreatment ($I(1,1,1)/I(2,0,0) \simeq 0.4$). Moreover, the role of this mechanism on the carbonation of polycrystalline CaO may be overruled by the influence of crystal imperfections. Thus, no effect of pretreatment on the carbonation reactivity would be foreseeable in this regard. Nonetheless, the preference for $CaCO_3$ nucleation in CaO (1,1,1) oriented surfaces is a potentially governing mechanism to bear in mind for the analysis of CaO conversion results.

Following an extensive series of experimental measurements on the specific surface area (S) of CaO derived from limestone calcination as a function of time, CO2 concentration in the calcining atmosphere, and temperature [41], the coherent crystal length L (nm) can be correlated to S (m^2/g) by means of the empirical equation $L = 74.5 - 46.5 \log S$. Interestingly, this equation suggests that surface area reduction in CaO is mainly caused by

crystallite growth (and not merely due to crystallite agglomeration and closure of pores) as early claimed by Anderson et al. [42, 43] from results a correlation between surface area reduction and crystal growth of CaO powders calcined in the presence of H_2O. In our work, BET surface area measurements were performed by N_2 sorption at 77 K on limestone samples calcined in a separate oven at similar conditions to those employed for in-situ calcination DRX analysis. The results obtained were S =6.2 m^2/g (raw limestone), S =6.3 m^2/g (milled limestone) and 9.4 m^2/g (annealed limestone) for which the above equation would yield a variation of the coherent crystal length between $L \simeq$40nm for CaO derived from raw and annealed limestone and $L \simeq$30 nm for CaO derived from milled limestone, which is in close agreement with the results directly inferred from the XRD spectra (Fig. 5). On the other hand, the similarity of these values allows foreseeing a not marked effect of pretreatment on the value of conversion in the fast carbonation phase of the first cycle.

C. Particle size distribution and mechanical strength analysis

Figure 6 shows the PSDs obtained for samples of raw, milled, and thermally annealed limestone dispersed in a liquid before and after ultrasonication. As may be seen, a quite broad dynamic range (between 0.2 and 2000 μm) is covered since the method of laser diffraction is a volume-based technique [44], thus allowing us to identify any effect of pretreatment and ultrasonication consisting of either particle growth or fragmentation. PSDs of the original (non ultrasonicated) samples indicate that both milling (Fig. 6b) and thermal annealing (Fig. 6c) induce an increase of the effective particle size, which can be attributed to the expected cold welding and sintering phenomena induced by these treatments. If the powder has been subjected to a heat pretreatment large aggregates may be formed due to material sintering, which causes joining of primary particles by strong chemical bonds [45]. On the

other hand, large compaction and shear forces generated during milling between particles trapped whenever two grinding balls collide can lead either to aggregation by cold welding or fragmentation depending on the material physical properties and milling operating conditions [46]. Accordingly, it may be observed that, in the case of ball milling, there is also a relative increase in the population of very fine particles that would be produced by fragmentation whereas, in the case of the thermally annealed sample, sintering yields a decrease of the population of small particles.

The effect of high energy ultrasonic irradiation on the PSDs indicate a relevant influence of pretreatment on the mechanical strength of the particles. Ultrasonication of the milled limestone sample leads to a remarkable population of very fine fragments. Conversely, the PSD of the ultrasonicated sample that was subjected to heat treatment is shifted to larger particle sizes as compared with the raw limestone. As well known from fracture mechanics studies on brittle materials, theoretical surface fracture energies (determined by the bond strength of the material) are systematically lower than the experimentally measured ones, which is due to the presence of randomly distributed flaws or cracks in the solid [47, 48]. The strength of a given particle is thus really determined by the weakest crack. Our results indicate that the structural damage caused by milling promotes friability, which is thus attributable to the increased density of defects in the solid as inferred from the microscopy and XRD analyses. Conversely, severe sintering during thermal annealing would lead to a decrease in the density of structural defects, which effectively increases the mechanical strength of the particles.

D. CaO multicyclic (c/r/c) conversion

Figure 7 shows the evolution of sample weight % obtained from the TG tests for samples of raw, milled and thermally annealed limestone during the 1st, 4th, and 13th carbonation/recarbonation/calcination (c/r/c) cycles. As well documented in the literature, it is seen that the carbonation stage (650°C, 15% vol CO_2) is started by a fast phase followed by a much slower diffusion controlled phase. Fast carbonation occurs approximately at the same rate and up to the same level in the 1st cycle for the three samples, which is consistent with the similar values of BET surface area obtained for the calcined samples. On the other hand, the subsequent slow phase in the carbonation stage undergoes at neatly different rates for the three samples since diffusive carbonation is determined by the crystal structure, which is affected by pretreatment. The next recarbonation stage, carried out at a higher temperature and high CO_2 concentration (800°C, 90% vol CO_2), exhibits likewise both a fast and a slow phase (see Fig. 7a inset). Remarkably, this observation is consistent with the recently proposed mechanism for product layer formation and growth, according to which $CaCO_3$ nucleates on the CaO surface in islands with a critical size determined by temperature-controlled surface diffusion [36, 49]. Since surface diffusion starts to be notable at temperatures near the Huttig temperature ($T_H \simeq 690$°C for CaO and 260°C for $CaCO_3$), it will be expectedly intense at the recarbonation temperature (800°C) of our tests. Thus, even though carbonation at 650°C evolved already in the slow phase, an increase of temperature up to 800°C would allow the formation of larger islands leaving fresh CaO surface exposed for fast CO_2 chemisorption in the initial phase of recarbonation. Note however that the initial fast recarbonation phase is rather short (inset of Fig. 7a). Arguably, this is due to the high CO_2 concentration, which leads to a quick depletion of CaO surface newly ex-

posed by the increase of temperature. An interesting feature observed in Fig. 7a is that, in contrast with fast carbonation, fast recarbonation does depend on the crystal structure. It occurs at a relatively high rate for the milled limestone, which would be caused by defects in the surface structure accelerating island growth by facilitating surface diffusion, whereas the opposite behavior is found for the thermally annealed sample in accordance with its higher degree of crystallinity that hinders surface diffusion. In regards to the rate of recarbonation in the subsequent slow phase it is also influenced by the crystal structure, which inidicates the control of lattice diffusion over carbonation in this phase. Importantly, the enhancement of recarbonation for the milled sample gives rise to an increase of the carbonation level in the fast phase of subsequent cycles whereas it is otherwise for the thermally annealed sample (as seen in Fig. 7b). This shows an important effect of crystal-structure controlled diffusion on the multicyclic CO_2 fast capture capacity. By intensifying diffusive carbonation the CaO skeleton left behind by CO_2 upon calcination is provided with a higher porosity and surface area available for fast carbonation. As the number of cycles builds up this beneficial effect is however progressively lost (Fig. 7c) in agreement with the XRD results suggesting that successive recarbonations erase the footprint of pretreatment on the crystal structure.

Conversion data in the fast and slow phases of the carbonation stage (X_{KN} and X_{DN}, respectively) and in the recarbonation stage (X_{RN}) are plotted in Fig. 8 as a function of the cycle number. As previously inferred, enhanced recarbonation in the 1st cycle for the milled limestone serves to promote fast conversion in subsequent cycles (Fig. 8a). Nevertheless, milling would lead also to an increase of the sintering rate by lattice diffusion in the calcination stage [37], which would be responsible for the relatively steeper loss of fast conversion with the cycle number observed for the milled sample (Fig. 8a). Moreover, enhanced lattice diffusion would contribute to reduce the density of structural defects as inferred from the

XRD analysis (indicating an increase of the coherent crystal length after recarbonation), which would lessen diffusive carbonation with the cycle number as demonstrated in Figs. 8b and 8c). In regards to the thermally annealed limestone, slow carbonation in the carbonation stage and carbonation in the recarbonation stage are impaired (Figs. 8b and 8c) as might be expected from the initially higher degree of crystallinity of this sample that would hinder diffusion. Recarbonation would be thus less efficient in regenerating the renovated CaO surface area. Thus, lower values of fast conversion in the carbonation stage are observed as compared to the raw limestone (Fig. 8a) in spite that a lower degree of sintering during calcination by lattice diffusion would be also foreseeable. Remarkably, Figs. 8b and Figs. 8c show an increase of X_{DN} and X_{RN} with the cycle number for the raw and thermally annealed samples in the first cycles, which is specially marked for the latter. A reactivation of diffusion controlled carbonation might be attributed to the loss of crystallinity of these samples after the 1st recarbonation as derived from the XRD analysis. Reactivation of diffusive carbonation is not observed in the case of milled limestone for which, according to the XRD analysis, crystallinity would be increased after recarbonation giving rise to a marked drop of X_{DN} and X_{RN} with the cycle number.

1. Long-term multicyclic conversion behavior

The evolution of CaO conversion in long series of carbonation/calcination cycles can be described by the equation

$$\frac{X_N}{X_1} = \frac{1 + b\,(N-1)}{1 + a\,(N-1)}; \qquad (N = 1, 2...) \tag{1}$$

which has been derived elsewhere [22] for CaO (not subjected to heat pretreatment) from the balance of surface area loss/gain in each cycle at a rate which is gradually reduced with the cycle number. Here a is the so-called sintering factor arising from the loss of surface area as a result of sintering in the calcination stage whereas b is the so-called regeneration factor, which reflects the gain of surface area stemming from diffusive carbonation. After a large number of cycles conversion would converge towards a residual value ($X_N \simeq X_r = X_1(b/a)$ for $N >> 1$). Typically, it is $b << a$ for limestone derived CaO since diffusive carbonation is negligible whereas sintering of the CaO skeleton is rather significant at ordinary carbonation/calcination (c/c) CaL conditions [22]. Consequently, CaO residual conversion turns out to be very low. The introduction of a recarbonation stage in between carbonation and calcination (c/r/c cycles) would enhance the regeneration of a porous CaO skeleton by intensifying diffusive carbonation thus leading to an increase of the residual conversion. This is seen in Fig. 9 where conversion data (at the end of the carbonation stage) are plotted for the raw, milled and thermally annealed limestones subjected to 50 c/r/c cycles. Data obtained for the raw limestone subjected to c/c cycles are also shown for comparison. Solid lines shown in Fig. 9 are drawn from the best fits of the data to Eq. 1. Residual conversion inferred for the raw limestone subjected to c/c cycles is $X_r \simeq 0.1$, which is similar to the typical value reported for a wide variety of natural limestones [13, 15]. On the other hand, the residual conversion obtained for raw limestone subjected to c/r/c cycles is increased up to $X_r \sim 0.25$. Values of residual conversion derived for the milled and thermally annealed limestones are slightly lower ($X_r \simeq 0.2$ and $X_r \simeq 0.24$, respectively), which is explainable from their diverse crystal structure. In the former case, a reduction of crystallinity degree would enhance diffusion but also promotes sintering, which leads to higher values of conversion in the first cycles at the expense of a greater deactivation rate. Contrarily, thermal

annealing would hinder sintering by lattice diffusion but recarbonation is impaired, which lessens the efficiency of this stage to regenerate the CaO surface area. Note also that Eq. 1 provides very good fits to conversion data on c/r/c cycles ($Rsqr \geqslant 0.9995$) as compared to the fit of the data on c/c cycles ($Rsqr \geqslant 0.983$). This suggests that the c/r/c process conforms quite accurately to the physical mechanism based on a sintering/regeneration balance that was proposed to derive Eq. 1 [22]. On the other hand, the surface area available for fast carbonation at each cycle in the c/c cycles would correspond essentially to that of the initial CaO skeleton that sinters (without appreciable regeneration) progressively with the cycle number at a decreasing rate as its surface area approaches a residual value. Accordingly, conversion of CaO samples subjected to c/c cycles would be better described from the empirical general power law expression (GPLE)

$$-\frac{d}{dt}\frac{S}{S_0} = k\left(\frac{S}{S_0} - \frac{S_r}{S_0}\right)^m \tag{2}$$

which was originally derived to fit data on the sintering induced loss of surface area suffered by supported metal catalysts for integer values of m =1,2 or 3 (first, second or third order processes, respectively) depending on the prevalent sintering mechanism [50, 51]. Here S is the surface area (taking an initial value S_0 and a residual value $S \simeq S_r$ for long sintering times t) and k is the so-called deactivation constant. Assuming that CaO conversion at each cycle is proportional to the surface area, whose decay conforms to Eq. 2 it is readily obtained after integration [52]

$$\frac{X_N}{X_1} = \frac{X_r}{X_1} + \left[\frac{1}{k(N-1)(m-1) + (1 - X_r/X_1)^{1-m}}\right]^{1/(m-1)}; \quad (N = 1, 2...) \tag{3}$$

Equation 3, with $m = 2$, was firstly proposed in [13] as a good fit to most of multicyclic c/c data for raw limestones leading to predicted residual values of conversion between 0.07

and 0.08. Note that for $m = 2$, Eq. 3 and Eq. 1 are formally equivalent expressions ($X_r = X_1(b/a)$, $k = a^2/(a-b)$) even though they are derived from diverse physical mechanisms. However, Eq. 3 provides the best fit to our c/c multicyclic data using $m = 3$ ($Rsqr \geqslant 0.993$ for $m = 3$ vs. $Rsqr \geqslant 0.983$ for $m = 2$, see inset of Fig. 9) in accordance to a third order sintering process. In the context of catalysts deactivation by sintering a third order process would be consistent with a sintering mechanism determined by atomic migration controlled by diffusion within the crystalline lattice [50, 51] whereas a second order process would in principle imply crystallite migration over the support surface followed by collision and coalescence even though some controversy is found in the related literature since sintering may involve more than one mechanism occurring simultaneously [53]. This improved fit predicts however a residual value of conversion close to zero in contrast with data from tests on some natural limestones carried out up 1000 c/c cycles and revealing the existence of a finite value of residual conversion [13, 15, 54]. On the other hand, conversion values are reported as low as 0.01 for limestones deeply sintered after calcination at very high temperatures and for extended period of times (see for example Fig. 7 in [55] and Fig. 10 in [14]). Interestingly, Lysikov et al. [14] reports multicyclic c/c data which are also better fitted by an equation similar to Eq. 3 using $m \simeq 3$ and giving residual values of conversion close to zero similarly to our observation. In particular, multicyclic tests on monocrystal-derived samples reported in [14] yield values of conversion after more than 200 cycles of about 0.03, which are much smaller than those obtained for polycrystalline samples (see Fig. 3 in [14]). Likewise, a close look at some data reported in [13] reveals that a third order process would improve the second order process fittings (see for example data in Fig. 9 for c/c cycles carried out under a very high calcination temperature). A likely mechanism which is worth further investigation is that the crystal structure is altered by deep sintering

promoting crystal growth along more stable (1,0,0) CaO oriented surfaces (less favorable to $CaCO_3$ nucleation) at the expense of the active (1,1,1) oriented surfaces. This would lead in some cases to extremely low values of multicyclic c/c conversion, which can be avoided as shown in our work by introducing a recarbonation stage that significantly regenerates the CaO skeleton through enhanced diffusive carbonation.

E. SEM/particle size analysis of cycled samples

SEM and physisorption analysis reported elsewhere [56] on natural limestones subjected to c/c cycles in a pilot-scale CaL setup (calcination at 850°C in air similarly to our TGA tests) indicate that the sorbent suffers a progressive reduction of microporosity accompanied by a parallel increase of mesoporosity as it is cycled. After only 6 c/c cycles the average pore size was observed to increase up to about 500 nm [56]. Representative SEM images of raw, milled and thermally annealed samples after being subjected to 50 c/r/c cycles in our tests (ending with a calcination stage) are displayed in Fig. 10. As can be seen in Fig. 10a, the c/r/c cycled raw limestone exhibits a marked presence of pores of typical size in the range 100 - 200 nm. Even though the small amount of mass employed in multicyclic TGA tests ($\sim$10 mg) prevents us from analyzing the cycled samples by physisorption, the relatively small size of the pores observed in the SEM pictures for the raw limestone subjected to 50 c/r/c cycles (Fig. 10a) upholds the argument that the introduction of an intermediate recarbonation stage mitigates the progressive increase of pore size as the sorbent is cycled. According to physisorption measurements of c/c cycled samples (reported in [56]), pores of size similar to the observed ones in Fig. 10a would result after calcination of the 1st c/c cycle, which suggests that recarbonation is quite effective in regenerating the pore skeleton even after 50 c/r/c cycles. It remains thus to be explained why the carbonation activity

still decays with the cycle number despite of the highly efficient regeneration of the sorbent pore skeleton by recarbonation. On the other hand, SEM images of the c/r/c cycled milled and thermally annealed samples (Fig. 10b and 10c) evidence a scarce presence of pores while cracks likely caused by thermal stresses are clearly visible in the SEM images of these samples. Extensive cracks are particularly remarkable in images of the thermally annealed sample (Fig. 10c), where the rarely observed pores are quite large (of size ~ 500 nm). SEM pictures demonstrate therefore a significant influence of pretreatment on the texture of the surface still persisting after 50 c/r/c cycles.

PSDs of samples after being subjected to the c/r/c cycles are shown in Fig. 11 as affected by high energy ultrasonic irradiation. As may be seen, large particles caused by either cold welding or sintering during milling and thermal annealing (Figs. 6b and 6c) are not observable in the cycled samples. This indicates that the strength of these large particles produced by pretreatment is decreased after cycling as to be disrupted by hydrodynamic stresses caused just by the stirring and pumping action of the predispersing unit in the instrument. On the other hand, the population of very small particles in the milled sample is decreased probably because of sintering of the small fragments during cycling (it is well established that milling of solids helps sintering at high temperatures by promoting lattice diffusion [27]). Ultrasonic irradiation yields a decrease of particle size as seen in Fig. 11, which is yet less marked than for the non-cycled samples. Note that the shift of the PSDs towards smaller particle sizes is more noticeable for the pretreated samples and particularly for the thermally annealed limestone, which is attributable to the development of cracks on the particles as observed in the SEM images of the cycled samples (Fig. 10b and 10c). As a result, the PSDs of the cycled samples subjected to high energy ultrasonic irradiation adjust to a similar distribution regardless of pretreatment. Thus, even though heat pre-

treatment/milling leads to an increase/decrease the mechanical strength of the limestone particles before the cycles, the effect of pretreatment on the mechanical strength of the sorbent would be blurred as the samples are subjected to a large number of cycles.

IV. CONCLUSIONS

This work analyzes the role of crystal structure as affected by milling and thermal annealing on the multicyclic CO_2 capture of limestone samples subjected to carbonation/recarbonation/calcination cycles, which is of practical interest in order to assess the efficiency of the CaL technology from process simulations and economic analysis. The introduction of a recarbonation stage in between ordinary carbonation and calcination stages serves to intensify diffusive carbonation, which would lead upon calcination to a regenerated CaO skeleton with promoted surface area and therefore increased fast carbonation activity. Our results demonstrate that the multicyclic CaO conversion in this novel CaL concept is critically affected by the crystal structure of the sorbent, which determines solid-sate diffusion. The loss of crystallinity induced by milling promotes diffusion in the recarbonation stage, which leads to higher CaO conversion in the fast carbonation phase of the first cycles. Yet, milling also favors lattice diffusion in the calcination stage, which gives rise to a higher deactivation rate. On the other hand, the crystallinity degree is increased by thermal annealing, which would mitigate sintering by lattice diffusion but on the other hand impairs diffusive carbonation in the recarbonation stage. A remarkable observation is that the recarbonation stage is initiated by a fast phase determined by the crystal structure, which indicates that this phase is governed by surface diffusion. This result is consistent with a recently proposed mechanism for the growth of $CaCO_3$ product layer on the CaO surface in islands ruled by surface diffusion. Thermal annealing and milling have a further relevant

effect on the mechanical strength of the particles as seen in our work from measurements of the particle size distribution of samples subjected to high energy ultrasonic irradiation. Thermal annealing hardens the solid whereas milling favors fragmentation. Nonetheless this effect is erased after multiple cycles, which is related to the development of cracks on the surface of the thermally pretreated sorbent (as shown by SEM images) that weakens the solid whereas on teh other hand promoted sintering in the milled sample would contribute to harden the particles after cycling. Likewise, the effect of pretreatment on the solid crystal structure and multicyclic CaO conversion is progressively blurred as the number of cycles is increased. Therefore, it may be concluded that the solid crystal structure is a determinant factor to be taken into account for assessing the efficiency of the CaL technology with a particular importance in the case that a recarbonation stage is introduced in the process.

Our study suggests that a direction of future research aimed at increasing the efficiency of the novel CaL technology built on carbonation/recarbonation/calcination cycles would be to search for optimum recarbonation conditions and Ca-based sorbents to enhance diffusive carbonation whereas at the same time not impairing the sorbent mechanical hardness. It must be remarked however that due to technical limitations in thermogravimetric tests performed until now to validate the novel CaL concept the sorbent is cyclicly calcined in air for regeneration whereas the CO_2 partial pressure in the calciner is expected to be high in practice. It is well known that CaO sintering is greatly accelerated by the presence of CO_2 at high concentration during limestone calcination, which might be affected by recarbonation. Further tests should be carried out wherein regeneration is performed by calcination under CO_2 in order to better assess the effect of recarbonation on the multicyclic CaO conversion. The effect of the likely presence of other gases in the calcination atmosphere such as SO_2 and H_2O arising from oxy-combustion should be also considered.

V. ACKNOWLEDGEMENTS

This work was supported by the Andalusian Regional Government Junta de Andalucia (contracts FQM-5735 and TEP-7858) , Spanish Government Agency Ministerio de Economa y Competitividad and FEDER funds (contracts FIS2011-25161 and CTQ2011-27626. One of the authors (PESJ) is supported by the Juan de la Cierva program of the Spanish Ministerio de Economa y Competitividad. We gratefully acknowledge the Microscopy, Functional Characterization, and X-ray services of the Innovation, Technology and Research Center of the University of Seville (CITIUS) and in particular Dr. Francisco Varela for his valuable assistance.

---

[1] J. Blamey, E. J. Anthony, J. Wang, and P. S. Fennell, "The calcium looping cycle for large-scale CO_2 capture," *Prog. Energ. Combust. Sci.*, vol. 36, no. 2, pp. 260–279, 2010.

[2] S. E. Edwards and V. Materic, "Calcium looping in solar power generation plants," *Solar Energy*, vol. 86, no. 9, pp. 2494 – 2503, 2012.

[3] S. Chen, W. Xiang, D. Wang, and Z. Xue, "Incorporating IGCC and CaO sorption - enhanced process for power generation with CO_2 capture," *Applied Energy*, vol. 95, pp. 285 – 294, 2012.

[4] B. Arias, M. Diego, J. Abanades, M. Lorenzo, L. Diaz, D. Martinez, J. Alvarez, and A. Sanchez-Biezma, "Demonstration of steady state CO_2 capture in a 1.7 MWth calcium looping pilot," *International Journal of Greenhouse Gas Control*, vol. 18, pp. 237 – 245, 2013.

[5] R. Barker, "Reversibility of the reaction $CaCO_3$ =CaO+CO_2," *J. Appl. Chem. Biotechnol.*, vol. 23, pp. 733 – 742, 1973.

[6] G. Grasa, R. Murillo, M. Alonso, and J. C. Abanades, "Application of the random pore model to the carbonation cyclic reaction," *AIChE J.*, vol. 55, no. 5, pp. 1246–1255, 2009.

[7] S. K. Bhatia and D. D. Perlmutter, "Effect of the product layer on the kinetics of the CO_2-lime reaction," *AIChE Journal*, vol. 29, no. 1, pp. 79–86, 1983.

[8] Z. Sun, S. Luo, P. Qi, and L.-S. Fan, "Ionic diffusion through calcite ($CaCO_3$) layer during the reaction of cao and $\{CO_2\}$," *Chemical Engineering Science*, vol. 81, pp. 164 – 168, 2012.

[9] L. M. Romeo, Y. Lara, P. Lisbona, and A. Martinez, "Economical assessment of competitive enhanced limestones for CO_2 capture cycles in power plants," *Fuel Processing Technology*, vol. 90, no. 6, pp. 803 – 811, 2009.

[10] N. Rodriguez, M. Alonso, J. C. Abanades, A. Charitos, C. Hawthorne, G. Scheffknecht, D. Y. Lu, and E. J. Anthony, "Comparison of experimental results from three dual fluidized bed test facilities capturing CO_2 with CaO," *Energy Procedia*, vol. 4, pp. 393 – 401, 2011.

[11] R. H. Borgwardt, "Sintering of nascent calcium oxide," *Chem. Eng. Sci.*, vol. 44, no. 1, pp. 53–60, 1989.

[12] J. M. Valverde, P. E. Sanchez-Jimenez, A. Perejon, and L. A. Perez-Maqueda, "Constant rate thermal analysis for enhancing the long-term CO_2 capture of CaO at ca-looping conditions," *Applied Energy*, vol. 108, pp. 108 – 120, 2013.

[13] G. S. Grasa and J. C. Abanades, "CO_2 capture capacity of CaO in long series of carbonation/calcination cycles," *Ind. Eng. Chem. Res.*, vol. 45, no. 26, pp. 8846–8851, 2006.

[14] A. I. Lysikov, A. N. Salanov, and A. G. Okunev, "Change of CO_2 carrying capacity of CaO in isothermal recarbonation-decomposition cycles," *Ind. Eng. Chem. Res.*, vol. 46, pp. 4633 – 4638, 2007.

[15] J. Wang, V. Manovic, Y. Wu, and E. J. Anthony, "A study on the activity of CaO-based sorbents for capturing CO_2 in clean energy processes," *Applied Energy*, vol. 87, no. 4, pp. 1453 – 1458, 2010.

[16] A. Martinez, Y. Lara, P. Lisbona, and L. M. Romeo, "Energy penalty reduction in the calcium looping cycle," *International Journal of Greenhouse Gas Control*, vol. 7, pp. 74 – 81, 2012.

[17] P. Lisbona, A. Martinez, and L. M. Romeo, "Hydrodynamical model and experimental results of a calcium looping cycle for CO_2 capture," *Applied Energy*, vol. 101, pp. 317 – 322, 2013.

[18] Y. Lara, P. Lisbona, A. Martnez, and L. M. Romeo, "Design and analysis of heat exchanger networks for integrated ca-looping systems," *Applied Energy*, vol. 111, pp. 690 – 700, 2013.

[19] C. Salvador, D. Lu, E. Anthony, and J. Abanades, "Enhancement of CaO for CO_2 capture in an FBC environment," *Chemical Engineering Journal*, vol. 96, no. 1 3, pp. 187 – 195, 2003.

[20] B. Arias, G. S. Grasa, M. Alonso, and J. C. Abanades, "Post - combustion calcium looping process with a highly stable sorbent activity by recarbonation," *Energy Environ. Sci.*, vol. 5, pp. 7353 – 7359, 2012.

[21] M. E. Diego, B. Arias, M. Alonso, and J. C. Abanades, "The impact of calcium sulfate and inert solids accumulation in post-combustion calcium looping systems," *Fuel*, vol. 109, pp. 184 – 190, 2013.

[22] J. M. Valverde, "A model on the CaO multicyclic conversion in the Ca-looping process," *Chemical Engineering Journal*, vol. 228, p. 1195 1206, 2013.

[23] M. C. Romano, "Modeling the carbonator of a Ca-looping process for CO_2 capture from power plant flue gas," *Chemical Engineering Science*, vol. 69, pp. 257 – 269, 2012.

[24] L. M. Romeo, Y. Lara, P. Lisbona, and J. M. Escosa, "Optimizing make-up flow in a $\{CO_2\}$ capture system using CaO," *Chemical Engineering Journal*, vol. 147, no. 2-3, pp. 252 – 258,

2009.

[25] H. Schmalzried, *One- and Two-Dimensional Defects in Crystals*, pp. 43–60. Wiley-VCH Verlag GmbH, 2007.

[26] Q. Zhang, E. Kasai, H. Mimura, and F. Saito, "Effect of dry grinding on ion-exchange characteristics of synthetic mordenite," *Advanced Powder Technology*, vol. 5, no. 3, pp. 289 – 296, 1994.

[27] P. Heitjans and S. Indris, "Fast diffusion in nanocrystalline ceramics prepared by ball milling," *Journal of Materials Science*, vol. 39, no. 16-17, pp. 5091–5096, 2004.

[28] M. Liu and B. Evans, "Dislocation recovery kinetics in single-crystal calcite," *Journal of Geophysical Research: Solid Earth*, vol. 102, no. B11, pp. 24801–24809, 1997.

[29] A. K. Kronenberg, R. A. Yund, and B. J. Giletti, "Carbon and oxygen diffusion in calcite: Effects of Mn content and PH2O," *Physics and Chemistry of Minerals*, vol. 11, no. 3, pp. 101–112, 1984.

[30] T. F. Anderson, "Self-diffusion of carbon and oxygen in calcite by isotope exchange with carbon dioxide," *Journal of Geophysical Research*, vol. 74, no. 15, pp. 3918–3932, 1969.

[31] V. Manovic, J.-P. Charland, J. Blamey, P. S. Fennell, D. Y. Lu, and E. J. Anthony, "Influence of calcination conditions on carrying capacity of CaO-based sorbent in CO_2 looping cycles," *Fuel*, vol. 88, pp. 1893–1900, 2009.

[32] P. Sanchez-Jimenez, L. Perez-Maqueda, and J. Valverde, "Nanosilica supported cao: A regenerable and mechanically hard {CO2} sorbent at ca-looping conditions," *Applied Energy*, vol. 118, pp. 92 – 99, 2014.

[33] K. A. Kusters, S. E. Pratsinis, S. G. Thoma, and D. M. Smith, "Ultrasonic fragmentation of agglomerate powders," *Chem. Eng. Sci.*, vol. 48, no. 24, pp. 4119–4127, 1993.

[34] R. Wagterveld, L. Boels, and M. M. G. Witkamp, "Visualization of acoustic cavitation effects on suspended calcite crystals," *Ultrasonics Sonochemistry*, vol. 18, no. 1, pp. 216 – 225, 2011.

[35] D. R. Glasson, "Reactivity of lime and related oxides. xvi. sintering of lime," *J. Appl. Chem.*, vol. 17, p. 91 96, 1967.

[36] Z.-S. Li, F. Fang, X.-Y. Tang, and N.-S. Cai, "Effect of temperature on the carbonation reaction of CaO with CO_2," *Energy & Fuels*, vol. 26, no. 4, pp. 2473–2482, 2012.

[37] J. S. Forrester, H. J. Goodshaw, E. H. Kisi, G. J. Suaning, and J. S. Zobec, "Effect of mechanical milling on the sintering behaviour of alumina," *J. Aust. Ceram. Soc.*, vol. 44, no. 1, pp. 47 – 52, 2008.

[38] A. M. Kierzkowska, R. Pacciani, and C. R. Müller, "CaO-based CO_2 sorbents: From fundamentals to the development of new, highly effective materials," *ChemSusChem*, vol. 6, no. 7, pp. 1130–1148, 2013.

[39] D. Mess, A. F. Sarofim, and J. P. Longwell, "Product layer diffusion during the reaction of calcium oxide with carbon dioxide," *Energy & Fuels*, vol. 13, no. 5, pp. 999–1005, 1999.

[40] R. Besson and L. Favergeon, "Atomic - scale study of calcite nucleation in calcium oxide," *The Journal of Physical Chemistry C*, vol. 117, no. 17, pp. 8813 – 8821, 2013.

[41] C. Chen, C. Zhao, C. Liang, and K. Pang, "Calcination and sintering characteristics of limestone under O_2/CO_2 combustion atmosphere," *Fuel Processing Technology*, vol. 88, no. 2, pp. 171 – 178, 2007.

[42] P. J. Anderson and P. L. Morgan, "Effects of water vapour on sintering of MgO," *Trans. Faraday Soc.*, vol. 60, pp. 930–937, 1964.

[43] P. J. Anderson, R. F. Horlock, and R. G. Avery, "Some effects of water vapour during the preparation and calcination of oxide powders," *Proc. Br. Ceram. Soc.*, vol. 3, p. 33, 1965.

[44] "Detecting oversized particles in ceramic powders using the Mastersizer 2000," tech. rep., Malvern Instruments (application note), 2005.

[45] J. Hyeon-Lee, G. Beaucage, S. E. Pratsinis, and S. Vemury, "Fractal analysis of flame-synthesized nanostructured silica and titania powders using small-angle x-ray scattering," *Langmuir*, vol. 14, pp. 5751–5756, 1998.

[46] T. P. Yadav, R. M. Yadav, and D. P. Singh, "Mechanical milling: a top down approach for the synthesis of nanomaterials and nanocomposites," *Nanoscience and Nanotechnology*, vol. 2, pp. 22 – 48, 2012.

[47] S. Yashima, Y. Kanda, and S. Sano, "Relationships between particle size and fracture energy or impact velocity required to fracture as estimated from single particle crushing," *Powder Technol.*, vol. 51, no. 3, pp. 277–282, 1987.

[48] P. M. Amaral, J. C. Fernandes, and L. G. Rosa, "Weibull statistical analysis of granite bending strength," *Rock Mech. Rock Eng.*, vol. 41, pp. 917–928, 2008.

[49] Z. Li, H. Sun, and N. Cai, "Rate equation theory for the carbonation reaction of cao with CO_2," *Energy & Fuels*, vol. 26, no. 7, pp. 4607–4616, 2012.

[50] C. H. Bartholomew, "Sintering kinetics of supported metals: new perspectives from a unifying GPLE treatment," *Applied Catalysis A: General*, vol. 107, no. 1, pp. 1 – 57, 1993.

[51] C. H. Bartholomew, "Sintering kinetics of supported metals: Perspectives from a generalized power law approach," in *Catalyst Deactivation 1994 Proceedings of the 6th International Symposium* (B. Delmon and G. Froment, eds.), vol. 88 of *Studies in Surface Science and Catalysis*, pp. 1 – 18, Elsevier, 1994.

[52] J. M. Valverde, P. E. Sanchez Jimenez, A. Perejon, and L. A. Perez-Maqueda, "CO_2 multicyclic capture of pretreated/doped CaO in the Ca – looping process. Theory and experiments," *Phys.*

627 *Chem. Chem. Phys.*, vol. 15, pp. 11775 – 11793, 2013.

628 [53] C. H. Bartholomew, "Sintering and redispersion of supported metals: Perspectives from the
629 literature of the past decade," in *Catalyst Deactivation Proceedings of the 7th International*
630 *Symposium* (C. Bartholomew and G. Fuentes, eds.), vol. 111 of *Studies in Surface Science and*
631 *Catalysis*, pp. 585 – 592, Elsevier, 1997.

632 [54] Y. Chen, J. Yang, R. N. Dave, and R. Pfeffer, "Granulation of cohesive geldart group C pow-
633 ders in a mini-glatt fluidized bed by pre-coating with nanoparticles," *Powder Tech.*, vol. 191,
634 pp. 206 – 217, 2009.

635 [55] V. Manovic and E. J. Anthony, "Thermal activation of CaO-based sorbent and self-reactivation
636 during CO_2 capture looping cycles," *Environ. Sci. Technol.*, vol. 42, pp. 4170–4174, 2008.

637 [56] J. C. Abanades, E. J. Anthony, D. Y. Lu, C. Salvador, and D. Alvarez, "Capture of CO_2 from
638 combustion gases in a fluidized bed of CaO," *AIChE J.*, vol. 50, no. 7, pp. 1614–1622, 2004.

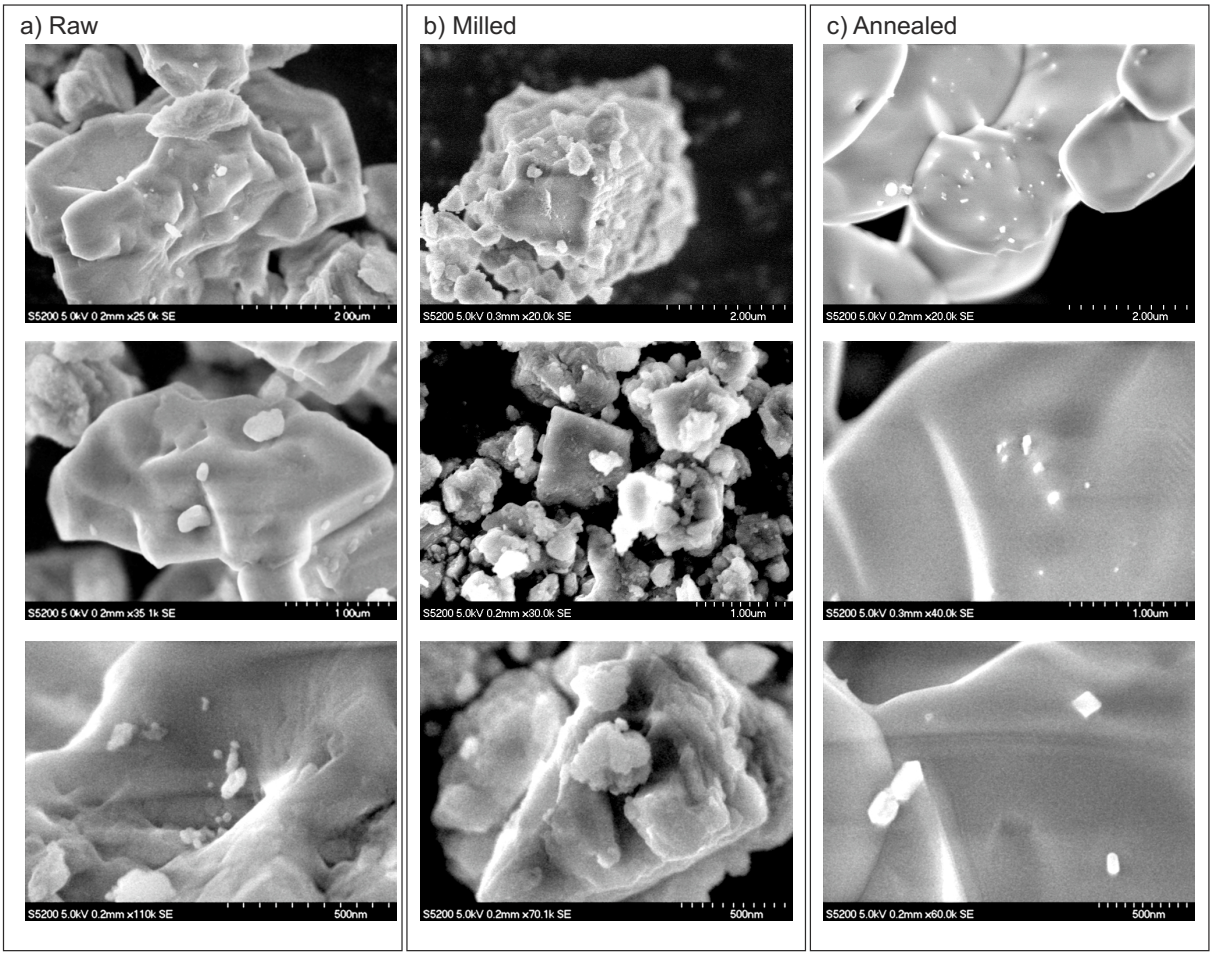

FIG. 1. Representative SEM pictures of raw, milled and thermally annealed limestone samples.

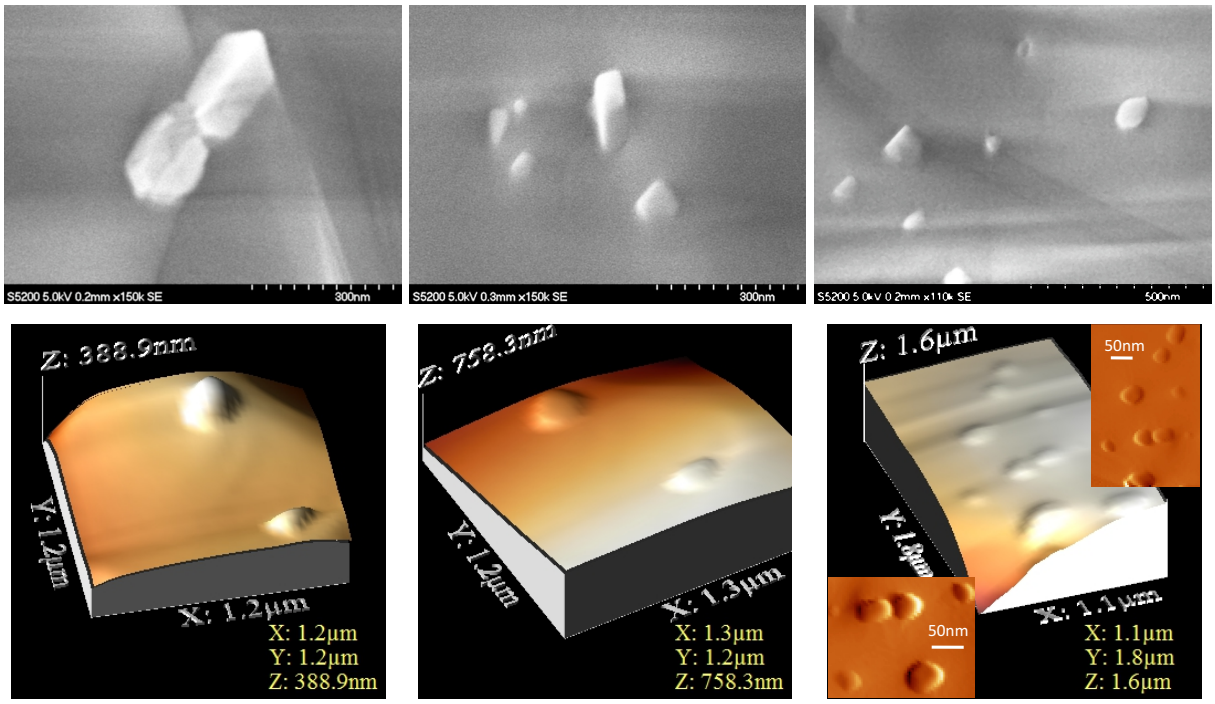

FIG. 2. SEM (top) and SPM (bottom) pictures of thermally annealed limestone particles showing in detail $CaCO_3$ nanocrystals grown on the surface of the particles during treatment.

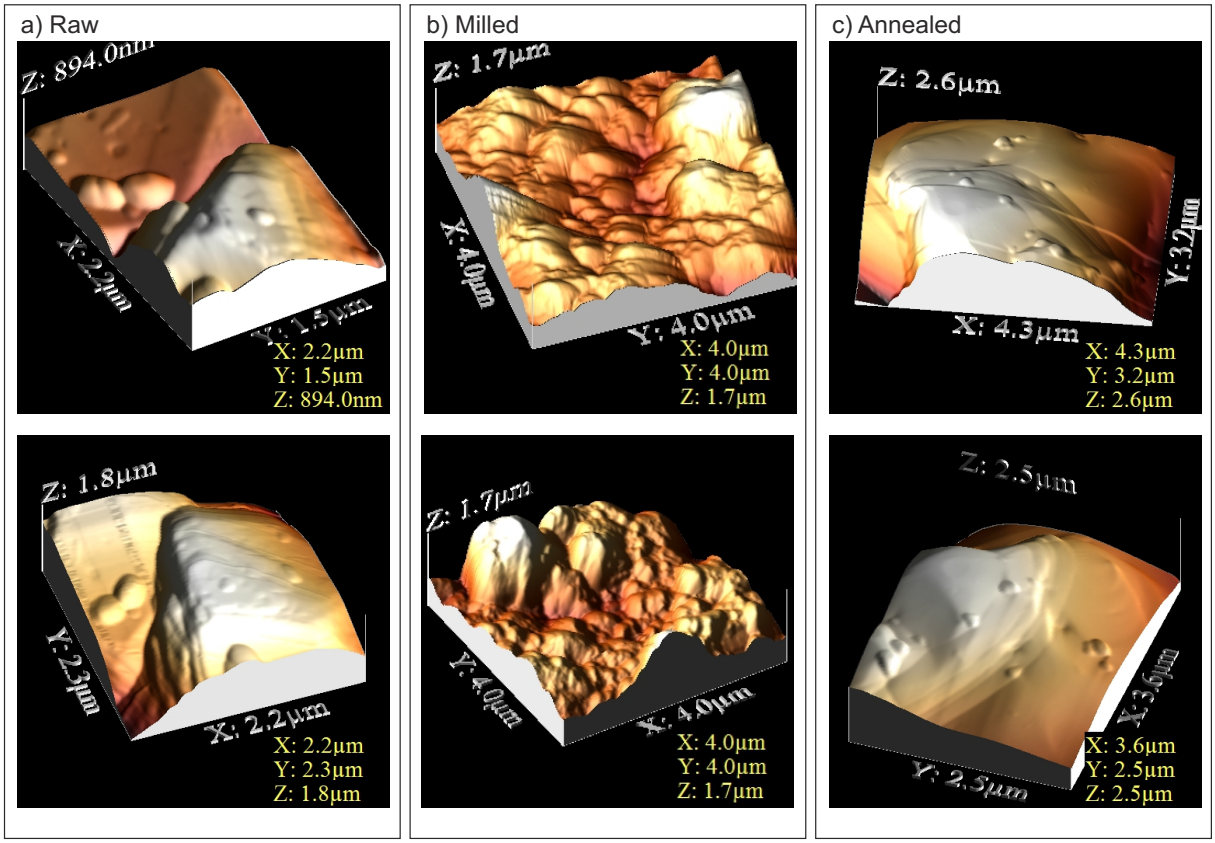

FIG. 3. Representative SPM pictures of raw, milled and thermally annealed limestone particles.

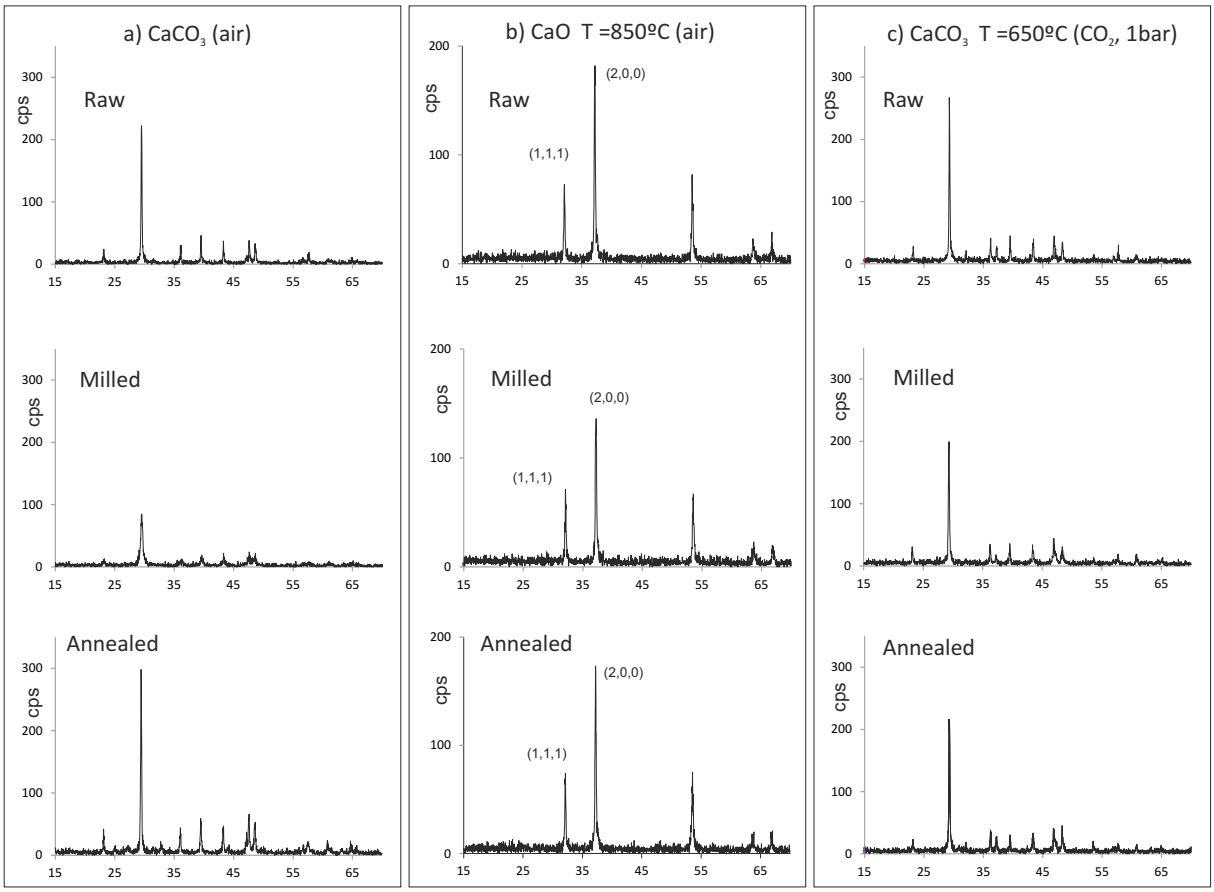

FIG. 4. XR diffractograms obtained for raw, milled and thermally annealed limestone samples in air at ambient temperature (a), after in-situ calcination at 850°C in air (b), and after in-situ carbonation at 650°C in CO_2 at 1bar (c). The peaks corresponding to crystal planes (1,1,1) and (2,0,0) for CaO derived by in-situ calcination are indicated.

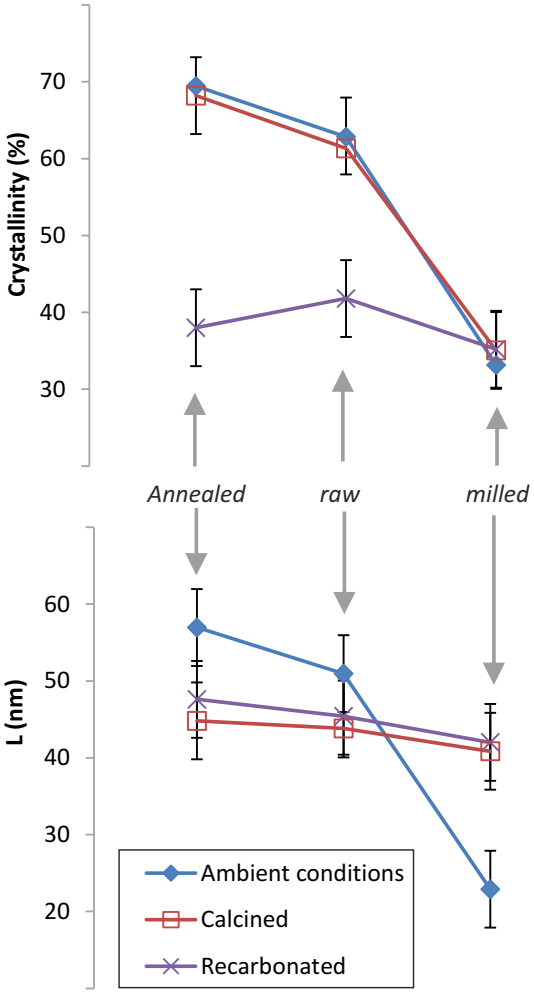

FIG. 5. Crystallinity % and coherent crystal length for raw, milled and thermally annealed limestone samples at ambient temperature, after in-situ calcination (850°C in air) and in-situ recarbonation (650°C in CO_2 at 1 bar). Each data point and error bar corresponds to the average value and scatter obtained from four independent measures.

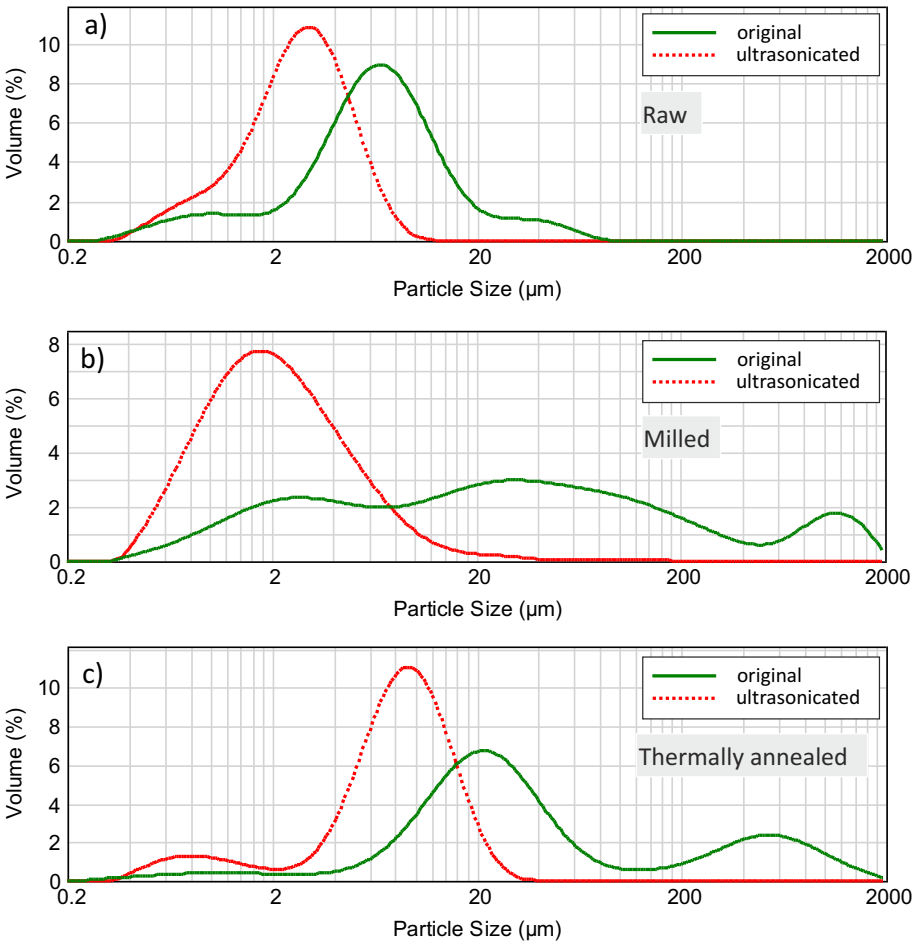

FIG. 6. Particle size distributions obtained by laser diffractometry of (a) raw, (b) milled and (c) thermally annealed limestone samples dispersed in 2-propanol and for dispersed samples pre-subjected to high energy ultrasonication. Each curve is obtained by averaging three independent measures showing low variability.

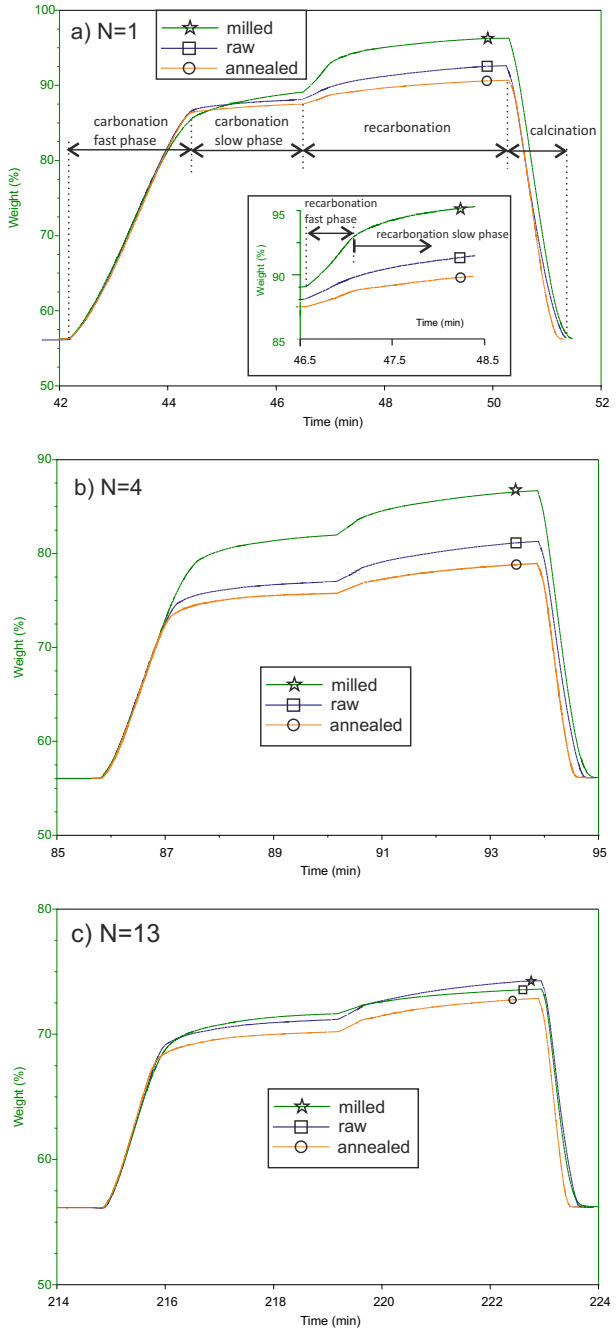

FIG. 7. Evolution of sample weight % obtained from TG tests on raw, milled and thermally annealed limestone samples during 1st (a), 4th (b), and 13th (c) carbonation/recarbonation/calcination cycles. Fast and slow phases of the carbonation stage, recarbonation stage and calcination stage of the 1st cycle are indicated in a). The inset of a) is a zoom of the recarbonation stage indicating the existence of fast and slow phases in this stage.

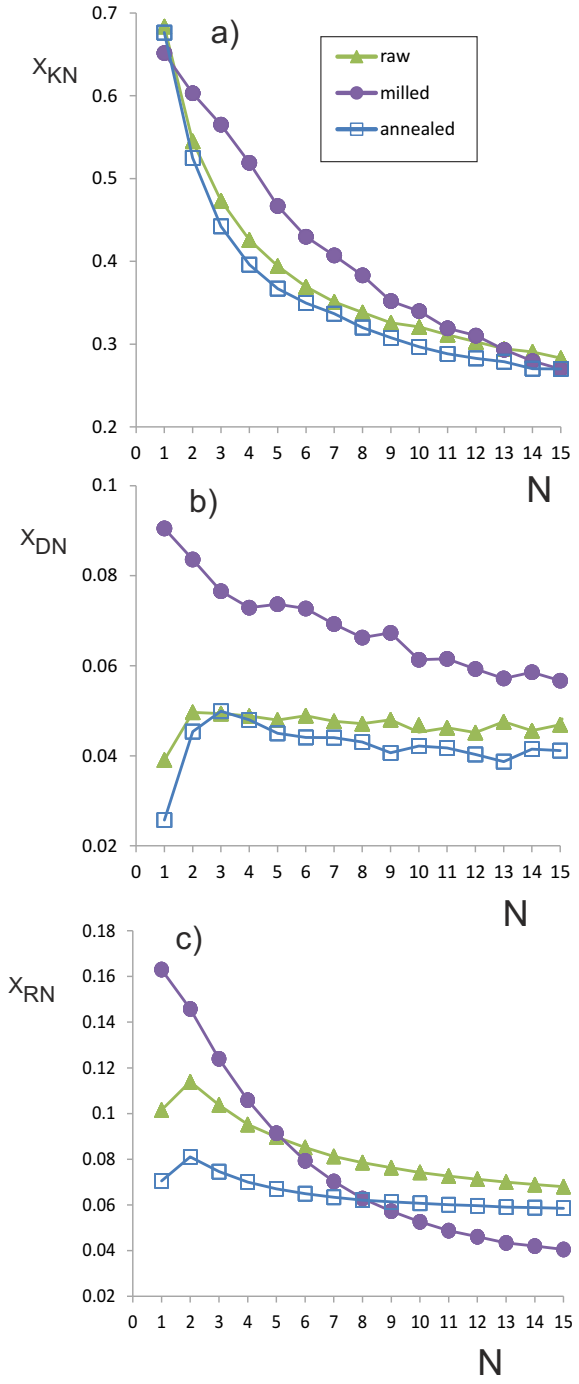

FIG. 8. a); b) Conversion in the fast and slow phases of the carbonation stage (X_{KN} and X_{DN}, respectively) for samples of raw, milled and thermally annealed limestones subjected to carbonation/recarbonation/calcination cycles. c) Conversion in the recarbonation stage X_{RN}.

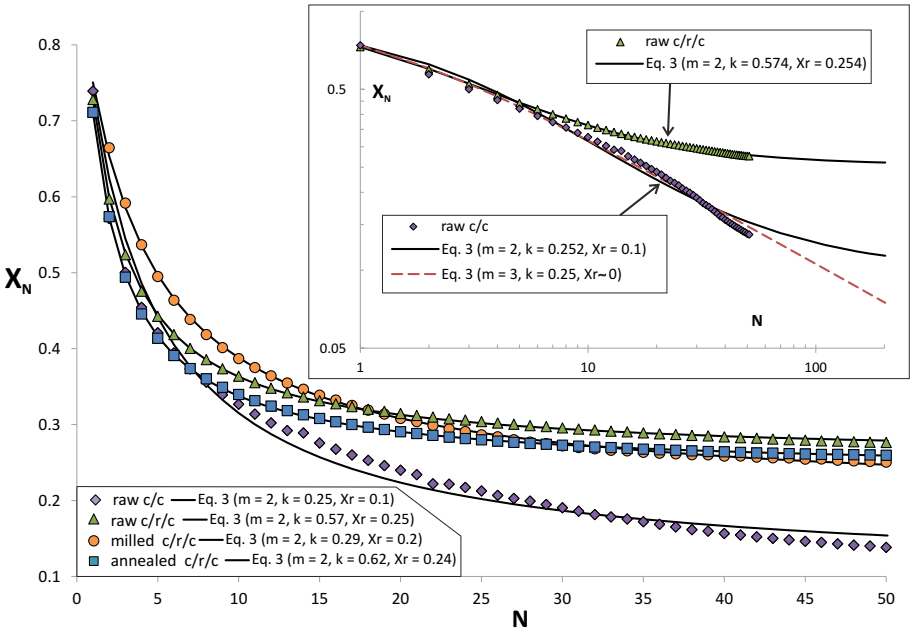

FIG. 9. Conversion at the end of the carbonation stage for samples of raw, milled and thermally annealed limestones subjected to 50 carbonation/recarbonation/calcination (c/r/c) cycles. Data from ordinary carbonation/calcination (c/c) cycles on raw limestone are also shown for comparison. The solid lines represent the best fit of the data to Eq. 1 (formally equivalent to Eq. 3 for $m = 2$). The inset shows data (log-log representation) on the raw limestone subjected to c/r/c and c/c cycles. Curves are plotted from the best fits of data to Eq. 3 according to second and third order sintering processes ($m = 2$ and $m = 3$, respectively) and extrapolated to large N.

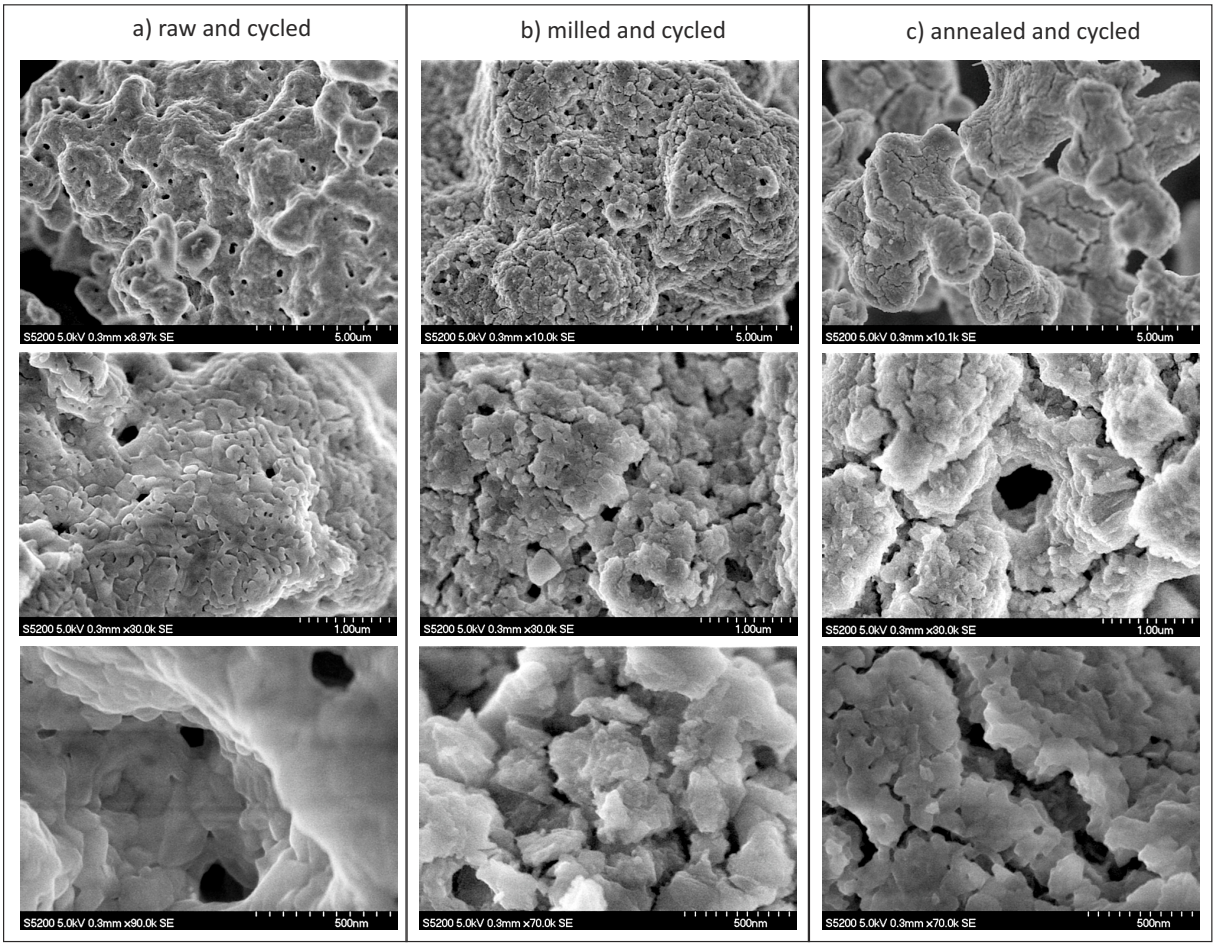

FIG. 10. Representative SEM pictures of raw (a), milled (b) and thermally annealed (c) limestone samples after being subjected to 50 carbonation/recarbonation/calcination cycles.

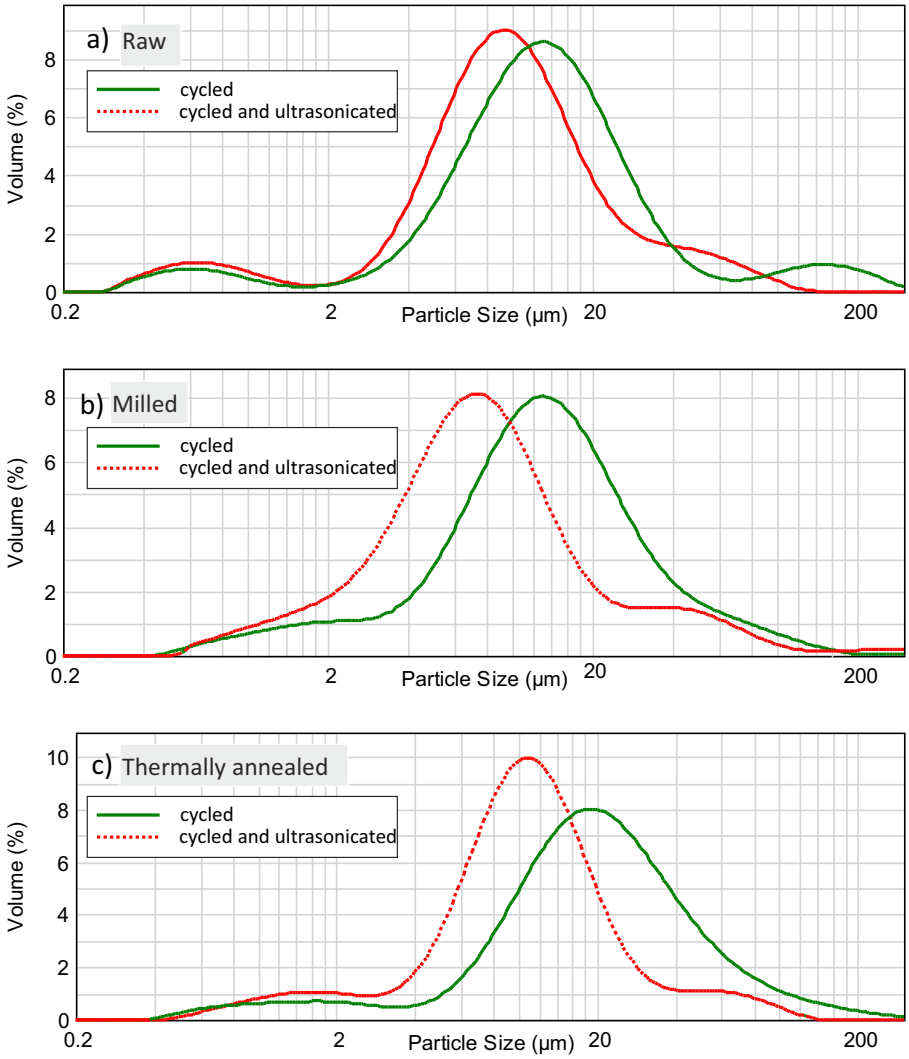

FIG. 11. Particle size distributions obtained by laser diffractometry of (a) raw, (b) milled and (c) thermally annealed limestone samples after being subjected to 50 carbonation/recarbonation/calcination cycles. Results are shown for cycled samples dispersed in 2-propanol and for cycled samples dispersed in 2-propanol and subjected to high energy ultrasonic irradiation. Each curve is obtained by averaging three independent measures showing low variability.